# Quantum computation in a Ising spin chain taking into account second neighbor couplings

G. V. López, T. Gorin and L. Lara

Departamento de Física, Universidad de Guadalajara,

Blvd. Marcelino García Barragan y Calzada Olímpica, C.P. 44480 Guadalajara, Jalisco, México

February 1, 2008

**Abstract**

We consider the realization of a quantum computer in a chain of nuclear spins coupled by an Ising interaction. Quantum algorithms can be performed with the help of appropriate radio-frequency pulses. In addition to the standard nearest-neighbor Ising coupling, we also allow for a second neighbor coupling. It is shown, how to apply the $2\pi k$ method in this more general setting, where the additional coupling eventually allows to save a few pulses. We illustrate our results with two numerical simulations: the Shor prime factorization of the number 4 and the teleportation of a qubit along a chain of 3 qubits. In both cases, the optimal Rabi frequency (to suppress non-resonant effects) depends primarily on the strength of the second neighbor interaction.

PACS: 03.67.-a, 03.67.Lx, 03.65.Ta, 03.67.Dd, 03.67.Hk

## 1 Introduction

The Ising-spin chain has been proposed in (Lloyd 1993, Berman et al. 1994, Lloyd 1995, Berman et al. 2001) as a theoretical system which allows to implement a quantum computer. Typically, one would think of a chain of spin-1/2 nucleons embedded into a solid crystal, as a possible physical system, whose dynamics may be well described by the Ising Hamiltonian. This system must be subjected to a magnetic field, constant in time, with a sufficently strong variation along the spin chain. Additional RF-pulses (radio-frequency pulses) then allow the coherent control of the state of the system such that a quantum protocol can be realized (Berman et al. 2000, Berman et al. 2001, Berman et al. 2002). This is a special form of

NMR quantum computation as described in (Jones 2000). Ultracold atoms in optical lattices may provide an alternative physical realization of a Ising-Hamiltonian (García-Ripoll and Cirac 2003).

Typically, in these system we find two types of dipolar interactions: (i) Intrinsic dipole couplings between the nuclear spins. Those scale as distance $r^{-3}$ and can be cancelled by the "magic angle" method (Slichter 1996). (ii) Mediated (mainly by the electrons) dipole couplings which have no clear distance dependence.

Up to now, this model has been developed just theoretically and hopefully the technological and experimental part may start in a near future. However, because the Hamiltonian of this system is well known, many theoretical studies have been made (Berman et al. 1994, Berman et al. 2000, Berman et al. 2001, Berman et al. $2002^{(a)}$, Berman et al. $2002^{(b)}$, Berman et al. $2002^{(c)}$, López et al. 2003, Celardo et al. 2005) which are also important for the general understanding of quantum computation. In this model, first neighbor Ising interaction among the nuclear spins of paramagnetic particles of spin one half was considered. Thus, in this paper we want to consider also second neighbor Ising interaction among the nuclear spins. The transverse coupling will be neglected since one could expect that their coupling constants to be a least two or three orders of magnitude smaller than the longitudinal coupling constant (Ising) for our particular configuration. With a register of 4 qubits, we perform a numerical simulation of Shor's factorization algorithm (Shor 1994) of the number 4 and teleportation (Bennett et al. 1993) of an arbitrary qubit in a chain of three qubits, allowing for an interaction between second neighbors in the system.

# 2 The model

We consider an Ising spin chain with nearest and next-nearest neighbor interaction as a model for a quantum register. The spin chain is subject to a constant external magnetic field in $z$-direction, as well as to RF-pulses (with the magnetic field vector in the x-y plane). This chain is inside a strong magnetic field in the z-direction and may be subject to RF-pulses (with the magnetic field vector in the x-y plane). The constant magnetic field $B(z)$, which must be extremely strong, also has a field gradient in the $z$-direction, which allows individual addressability of the qubits. During an RF-pulse, the whole external field may be written as

$$\boldsymbol{B} = (B_0 \cos(wt + \varphi), -B_0 \sin(wt + \varphi), B(z)) \,, \tag{1}$$

where $B_0$, $w$ and $\varphi$ are the amplitude, the angular frequency and the phase of the RF-field. They are assumed to remain constant during a pulse, but are typically chosen differently for

different pulses. Without any RF-field, the Hamiltonian reads:

$$H_0 = -\hbar \left( \sum_{k=1}^{n} w_k \, I_k^z + 2J \sum_{k=1}^{n-1} I_k^z \, I_{k+1}^z + 2J' \sum_{k=1}^{n-2} I_k^z \, I_{k+2}^z \right) , \tag{2}$$

where $w_k$ is the Larmor frequency of spin $k$. We denote with $|0_k\rangle$ the state where the nuclear spin $k$ is parallel to the magnetic field and $|1_k\rangle$ where it is anti-parallel. The RF-field induces the desired transitions between the Zeeman levels of the systems.

The structure of the Hilbert space of the spin chain is particularly appropriate for quantum information studies, where the basis unit of information is a two-level quantum system ("quantum bit", or qubit for short). Any such state $\Psi = C_0|0\rangle + C_1|1\rangle$ can be represented with respect to some basis stats $|0\rangle$ and $|1\rangle$ by two complex numbers $C_0$ and $C_1$ such that $|C_0|^2 + |C_1|^2 = 1$. The $L$-tensorial product of $L$-basic qubits form an $L$-register of $L$-qubits. In this space, we denote the resulting product basis by $|\alpha\rangle = |i_{L-1}, \ldots, i_0\rangle$ with $i_j = 0, 1$ for $j = 0, \ldots, L-1$. A pure wave function can be expanded in this basis by $\Psi = \sum C_\alpha |\alpha\rangle$, where $\sum_\alpha |C_\alpha|^2 = 1$s. For notational convenience, we require that $\alpha = \sum_{j=0}^{L-1} i_j \, 2^j$.

The Hamiltonian $H_0$ in Eq. (2) is diagonal in the computational basis (the product basis defined above):

$$\begin{aligned} H_0 \, |\alpha_{n-1} \ldots \alpha_1 \alpha_0\rangle &= E_\alpha \, |\alpha_{n-1} \ldots \alpha_2 \alpha_0\rangle \qquad I_k^z |\alpha_k\rangle = \frac{(-1)^{\alpha_k}}{2} |\alpha_k\rangle \\ E_\alpha &= -\frac{\hbar}{2} \left( \sum_{k=0}^{n-1} (-1)^{\alpha_k} \, w_k + J \sum_{k=0}^{n-2} (-1)^{\alpha_k + \alpha_{k+1}} + J' \sum_{k=0}^{n-3} (-1)^{\alpha_k + \alpha_{k+2}} \right) . \end{aligned} \tag{3}$$

The index $\alpha$ without subscript denotes the positive integer represented by the string $\alpha_{n-1} \ldots \alpha_1 \alpha_0$ in the binary number system, *e.g.*: $H_0 \, |101\rangle = E_5 \, |101\rangle$. Choosing the Larmor frequencies $w_k$ such that $\forall k \, : \, w_k / w_{k-1} = 2$, leads to a spectrum which (ignoring the spin-spin coupling terms) has equidistant levels: $E_\alpha - E_{\alpha-1} = \text{constant}$.

The RF-pulses are essential for any implementation of a quantum algorithm. During such a pulse, the full Hamiltonian may be written in the form

$$H = H_0 + W(t) \qquad W(t) = -\frac{\hbar \, \Omega}{2} \sum_{k=1}^{n} \left( \mathrm{e}^{\mathrm{i}(wt+\varphi)} \, I_k^+ + \mathrm{e}^{-\mathrm{i}(wt+\varphi)} \, I_k^- \right) , \tag{4}$$

where the frequency $w$, the phase-offset $\varphi$ and the Rabi frequency $\Omega$ are free parameters ($\Omega/\gamma$ is the amplitude of the RF field, where $\gamma$ is the nuclear spin gyromagnetic ratio). In the computational basis $|\alpha_{n-1} \ldots \alpha_1 \alpha_0\rangle$ the raising and lowering operators for spin $k$ can be written as: $I_k^+ = |0_k\rangle\langle 1_k|$ and $I_k^- = |1_k\rangle\langle 0_k|$. We will consider sequences of pulses, where each

pulse may vary in time. During the pulses $\varphi$ and $\Omega$ are fixed as well as the RF frequency $w$ which is assumed to be on resonance with some allowed transition. We assume that there are no degeneracies. Hence,

$$w = \frac{E_{\alpha|\alpha_k=1} - E_{\alpha|\alpha_k=0}}{\hbar} = w_k + J\left[(-1)^{\alpha_{k+1}} + (-1)^{\alpha_{k-1}}\right] + J'\left[(-1)^{\alpha_{k+2}} + (-1)^{\alpha_{k-2}}\right], \quad (5)$$

where it is understood that $(-1)^{\alpha_l} = 0$ if $l < 0$ or $l > n$. Thus, in the center of the spin chain (away from the borders) the $J$-coupling may lead to frequency shifts of $\Delta w = 0$ or $\pm 2J$ ($\Delta w' = 0$ or $\pm 2J'$), whereas at the borders the frequency shifts are $\Delta w = \pm J$ ($\Delta w' = \pm J'$). The following notation is based on these observations. The unitary evolution (in the interaction picture) during a resonant RF pulse is denoted by

$$R_k^{\mu,\nu}(\Omega\tau, \varphi) = \mathrm{e}^{-\mathrm{i}H_0\tau/\hbar}\, \mathrm{e}^{-\mathrm{i}H\tau/\hbar}\, \mathrm{e}^{\mathrm{i}H_0\tau/\hbar} \qquad w = w_k + \mu J + \nu J' \,, \quad (6)$$

with $\mu, \nu \in [-2, -1, 0, 1, 2]$. Note that in order that $R_k^{\mu,\nu}(\Omega\tau, \varphi)$ is a resonant pulse, the indices $\mu, \nu, k$ must fulfill certain relations as discussed above (*i.e.* not all combinations lead to resonant transitions). The wave function dynamics during such RF-pulses is computed numerically as sketched in App. A.

In the numerical simulations to follow (Secs. 4 and 5), we have chosen the following parameters in units of $2\pi\times$Mhz,

$$\omega_0 = 100\ ,\ \omega_1 = 200\ ,\ \omega_2 = 400\ ,\ \omega_3 = 800,\ J = 10\ ,\ J' = 0.4\ ,\ \Omega = 0.1\ . \quad (7)$$

These parameters give rise to a simple Zeeman spectrum with equidistant levels. For the possibly more realistic design described in (Berman et al. $2002^{(b)}$), we would expect similar results. In our simulations, we will take advantage of the second neighbor interaction in order to reduce the number of pulses for the realization of the quantum algorithms (López and Lara 2006). Those are Shor's factorization in Sec. 4 and teleportation in Sec. 5.

# 3 Second neighbor interaction and the $2\pi k$-method

For the considerations in the previous section, only resonant transitions have been taken into account. That allowed trivially to describe the dynamics under the RF-pulses analytically. However, it is possible to go beyond this simple picture. To that end we distinguish near resonant transitions where the frequency differs from the resonant frequency by values of the order of $J$ or $J'$ and far resonant transitions, where the difference is of the order of the Larmor frequencies. Then it can be shown that the Hamiltonian decomposes into independent 2x2 matrix blocks as long as far resonant transitions are neglected. This still allows to describe

the dynamics under the RF-pulses analytically, and in particular it allows to control and suppress the non (near) resonant transitions. The $2\pi k$-method (Berman et al. 2002$^{(a)}$) and its generalization (Berman et al. 2002$^{(c)}$) resulted from such considerations.

Assume we perform the pulse $R_1^{0,-1}(\Omega\tau,\varphi)$ in the 4-qubit quantum register. This pulse induces the resonant transitions

$$|0001\rangle \leftrightarrow |0011\rangle \qquad |0100\rangle \leftrightarrow |0110\rangle \tag{8}$$

at the frequency $w = w_1 - J'$. However, it also induces the near-resonant transitions at frequencies $w + \Delta$

$$\begin{aligned} |1001\rangle \leftrightarrow |1011\rangle \qquad & |1100\rangle \leftrightarrow |1110\rangle \quad : \quad \Delta = 2J' \\ & |0000\rangle \leftrightarrow |0010\rangle \quad : \quad \Delta = 2J \\ & |0101\rangle \leftrightarrow |0111\rangle \quad : \quad \Delta = -2J \\ & |1000\rangle \leftrightarrow |1010\rangle \quad : \quad \Delta = 2J + 2J' \\ & |1101\rangle \leftrightarrow |1111\rangle \quad : \quad \Delta = -2J + 2J' \end{aligned} \tag{9}$$

In the near resonant approximation, we may write down an evolution equation for each transition separately. To this end let $\alpha$ denote the first state of the transition pair (where $\alpha_1 = 0$) and $\beta$ the second (where $\beta_1 = 1$, $\forall k \neq 1 : \beta_k = \alpha_k$). Then we find for the wave function coefficients in the interaction picture (see App. A):

$$\partial_t\, D_\alpha(t) = \frac{\mathrm{i}\,\Omega}{2}\, \mathrm{e}^{\mathrm{i}(\Delta t+\varphi)}\, D_\beta(t) \qquad \partial_t\, D_\beta(t) = \frac{\mathrm{i}\,\Omega}{2}\, \mathrm{e}^{-\mathrm{i}(\Delta t+\varphi)}\, D_\alpha(t)\ . \tag{10}$$

The solution for the evolution operator is

$$\begin{aligned} \begin{pmatrix} D_\alpha(t) \\ D_\beta(t) \end{pmatrix} &= U(t)\ \begin{pmatrix} D_\alpha(0) \\ D_\beta(0) \end{pmatrix} \\ U(t) &= \begin{pmatrix} \mathrm{e}^{\mathrm{i}\Delta t/2} & 0 \\ 0 & \mathrm{e}^{-\mathrm{i}\Delta t/2} \end{pmatrix} \begin{pmatrix} \cos\frac{\Omega_\mathrm{e} t}{2} - \frac{\mathrm{i}\Delta}{\Omega_\mathrm{e}}\ \sin\frac{\Omega_\mathrm{e} t}{2} & \frac{\mathrm{i}\Omega}{\Omega_\mathrm{e}}\, \mathrm{e}^{\mathrm{i}\varphi}\ \sin\frac{\Omega_\mathrm{e} t}{2} \\ \frac{\mathrm{i}\Omega}{\Omega_\mathrm{e}}\, \mathrm{e}^{-\mathrm{i}\varphi}\ \sin\frac{\Omega_\mathrm{e} t}{2} & \cos\frac{\Omega_\mathrm{e} t}{2} + \frac{\mathrm{i}\Delta}{\Omega_\mathrm{e}} \sin\frac{\Omega_\mathrm{e} t}{2} \end{pmatrix}\ , \end{aligned} \tag{11}$$

where $\Omega_\mathrm{e} = \sqrt{\Omega^2 + \Delta^2}$. Hence, *e.g.* for a $\pi$-pulse $t = \tau = \pi/\Omega$ at the end of the pulse, and we may tune $\Omega$ such that any near resonant transition is switched off. This only requires that

$$\frac{\Omega_\mathrm{e}\tau}{2} = \frac{\pi\,\Omega_\mathrm{e}}{2\,\Omega} = \frac{\pi}{2}\sqrt{1 + \frac{\Delta^2}{\Omega^2}} = k\pi \quad \Leftrightarrow \quad \sqrt{1 + \frac{\Delta^2}{\Omega^2}} = 2\,k\ . \tag{12}$$

The $2\pi k$-method as presented here has two shortcomings. If there are several near-resonant transitions with different frequency shifts $\Delta$ it will be impossible, in general, to eliminate all

of them. Second, any near resonant transition also implies a phase rotation, which cannot be corrected by the method. In principle some of those shortcomings can be overcome at the expense of more complex pulse sequences, as shown in (Berman et al. 2002c).

For the numerical simulations in Secs. 4 and 5 we define the optimal Rabi frequency to eliminate a near-resonant transition with shift $\Delta$ during a $\pi$-pulse as

$$\Omega_{\Delta}^{(k)} = \frac{|\Delta|}{\sqrt{4k^2-1}} \,. \tag{13}$$

Note that for a $\pi/2$-pulse the corresponding optimal Rabi frequency is given by the same equation, but with $k$ replaced by $2k$.

# 4 Simulations of Shor's factorization algorithm of number four

An experimental realization of Shor's factorization algorithm has been demonstrated recently in (Vandersypen et al. 2001) using nuclear magnetic resonance. Following Shor's approach (Shor 1994) for factorizing an integer number $N$, one selects a $L+M$-register of the form $|x;y\rangle$, where $|x\rangle$ is the input register of length $L$, and $|y\rangle$ is the evaluation register of length $M$. The $y$-register is used to store the values of the periodic function $y(x) = q^x (\mathrm{mod}\ N)$, where the integer $q$ is chosen co-prime to $N$ (*i.e.* the greatest common divisor $\gcd(q,N)=1$). The algorithm is divided into three parts (Nielsen and Chuanf 2000, chapter 5). First, one creates the uniform superposition of all basis states in the $x$-register. Second, one chooses some co-prime number $q$ and computes the function $y(x) = q^x (\mathrm{mod}\ N)$ in the $y$-register. Third, one applies the inverse discrete Fourier transform to the $x$-register. After these steps, one measures the state in the $x$-register, which provides the information on the factors of $N$. For more details, we refer the interested reader to (Nielsen and Chuang 2000).

For factorizing the number $N=4$, two qubits in each register are sufficient ($L=M=2$). The only co-prime number of $N$ is $q=3$, and thus the period of the function $y(x) = 3^x (\mathrm{mod}\ 4)$ gives the factors of $N$. In the present case this period is $T=2$. Applying the procedure above to the initial state $\Psi_0 = |00;00\rangle$, one obtains after each of the three steps:

$$\Psi_1^{(\mathrm{ideal})} = \frac{1}{2}\big(\,|00;00\rangle + |01;00\rangle + |10;00\rangle + |11;00\rangle\,\big) \tag{14}$$

$$\Psi_2^{(\mathrm{ideal})} = \frac{1}{2}\big(\,|00;01\rangle + |01;11\rangle + |10;01\rangle + |11;11\rangle\,\big) \tag{15}$$

$$\Psi_3^{(\mathrm{ideal})} = \frac{1}{2}\big(\,|00;01\rangle + |00;11\rangle + |10;01\rangle + |10;11\rangle\,\big)\,. \tag{16}$$

The measurement on the $x$-register give us the states $|00\rangle$ or $|10\rangle$ ($x = 0$ or $x = 2$), which implies that the period of the function $y(x)$ is $T = 2$, as expected.

The following computation is performed in the interaction picture. Using the parameters from Eq. (7) and starting with the ground state of the system, $\Psi_0 = |0000\rangle$, we create $\Psi_1$ with the help of three $\pi/2$-pulses:

$$\Psi_1 = R_3^{-1,1}(\pi/2, \pi/2)\; R_3^{1,1}(\pi/2, \pi/2)\; R_2^{2,1}(\pi/2, \pi/2)\; \Psi_0 \; . \tag{17}$$

The evaluation of the function $y(x) = 3^x (\mathrm{mod}\ 4)$ in the $y$-register is carried out with four $\pi$-pulses:

$$\Psi_2 = R_1^{-2,-1}(\pi, \pi/2)\; R_1^{-2,1}(\pi, \pi/2)\; R_0^{1,-1}(\pi, \pi/2)\; R_0^{1,1}(\pi, \pi/2)\; \Psi_1 \; . \tag{18}$$

Finally, the discrete Fourier transformation in the $x$-register is obtained through five $\pi$-pulses:

$$\Psi_3 = R_2^{-2,-1}(\pi, \pi/2)\; R_0^{-1,-1}(\pi, -\pi/2)\; R_0^{-1,1}(\pi, \pi/2)\; R_2^{0,1}(\pi, -\pi/2)\; R_0^{-1,-1}(\pi, -\pi/2)\; \Psi_2 \; . \tag{19}$$

The final measurement consists in tracing out the $y$-register, and measuring the probabilities of finding the $x$-register in any of the possible basis states. In the present case, we would get

$$\langle 00|\varrho_x|00\rangle = \langle 10|\varrho_x|10\rangle = \frac{1}{2} \qquad \langle 01|\varrho_x|01\rangle = \langle 11|\varrho_x|11\rangle = 0 \; , \tag{20}$$

where $\varrho_x = \mathrm{tr}_y |\Psi_3\rangle\langle\Psi_3|$. This yields the expected period $T = 2$.

In what follows, we simulate the pulse sequence for Shor's algorithm with our model Hamiltonian of Eq. (4). The wave-packet evolution is carried out in the interaction picture using the parameters given in Eq. (7). In Fig. 1 we show the difference between the final state $\Psi_3$, obtained from the evolution with the full Hamiltonian $H(t)$, and the ideal final state $\Psi_3^{(\mathrm{ideal})}$. The latter is obtained from an evolution where only the resonant transitions have been taken into account. As deviation, we plot the real (red impulses) and imaginary (blue impulses) parts of the difference between the respective expansion coefficients $D_\alpha$ and $D_\alpha^{(\mathrm{ideal})}$ as a function of $\alpha$, which denotes the basis states, as explained below Eq. (3). We can see that by far the largest error consist in an accumulation of residual phases in the expansion coefficients of those basis stats which are expected to be populated in $\Psi_3^{(\mathrm{ideal})}$, *i.e.* $|0001\rangle$, $|0011\rangle$, $|1001\rangle$, and $|1011\rangle$. This can be deduced from the large imaginary parts errors, visible in Fig. 1. However, the probabilities of the states remain within their right value.

In order to quantify the deviation of the real evolution with $H(t)$ from the ideal one, where only resonant transitions are taken into account, we introduce a figure of merit, the fidelity (Peres 1984, Schumacher 1995, Gorin et al. 2006)

$$F = |\langle \Psi^{(\mathrm{ideal})}|\Psi\rangle|^2 \; , \tag{21}$$

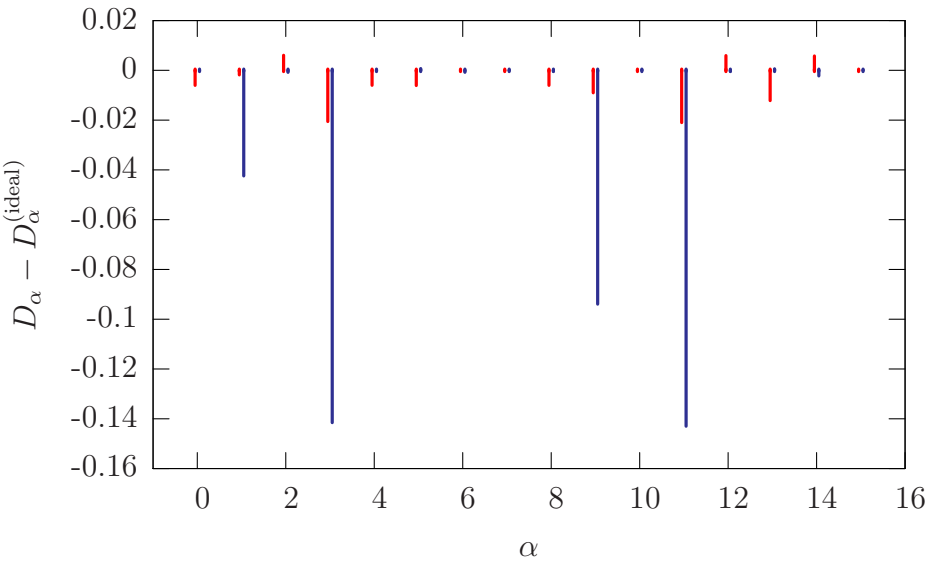


Figure 1: The difference in the expansion coefficients between the final state $\Psi_3$ obtained from the evolution with the full Hamiltonian and the ideal final state $\Psi_3^{(\mathrm{ideal})}$. Red impulses (towards the left) show the real part, blue impulses (towards the right) the imaginary part. The difference in the expansion coefficients is plotted versus $\alpha$, which labels the basis states.

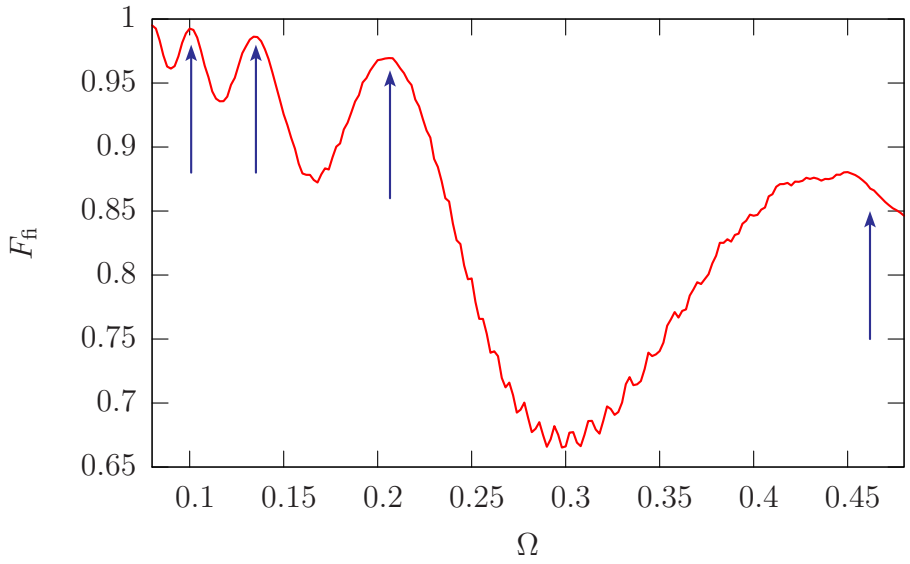


Figure 2: The fidelity, Eq. (21), for the final state resulting from the factorization algorithm as a function of the Rabi frequency $\Omega$. The blue arrows show the optimal Rabi frequencies $\Omega_\Delta^{(k)}$ according to Eq. (13), for $\Delta = 2J'$ and $k = 1, 2, 3$, and 4 (from right to left).

which gives the probability to find the system in the state $\Psi^{(\rm ideal)}$ even though it really is in the state $\Psi$. As we have seen in Sec. 3 that one can influence the accuracy of the implementation of the quantum protocol by appropriately choosing the Rabi frequency (the strength of the RF field) we will first investigate the dependence of the fidelity $F_{\rm fi} = |\langle\Psi_3^{(\rm ideal)}|\Psi_3\rangle|^2$ on the Rabi frequency. The result is shown in Fig. 2, where $F_{\rm fi}$ is plotted versus $\Omega$ in the interval $(0.08, 0.48)$. The blue arrows show the positions of the optimal Rabi frequencies $\Omega_\Delta^{(k)}$, according to Eq. (13) for $\Delta = 2J'$ and $k = 1, 2, 3$, and 4 (from right to left). The fidelity clearly behaves as expected. We find maxima for those values, where the $2\pi\,k$-relation is fulfilled. The resulting curve is rather smooth at small Rabi frequencies, while additional fast oscillations appear near $\Omega \approx 0.3$. The additional structures are due to the transitions where the detuning is of the order of $2J$. Since $J \gg J'$ these transitions have nearly no effect for small Rabi frequencies, but there effect becomes more and more significant as $\Omega$ increases. In practice, one would have to find a compromise between a sufficiently fast evolution (for that one needs large Rabi frequencies) and a sufficiently high fidelity, which can be achieved more easily at small Rabi frequencies.

In order to study the mechanism behind the $2\pi\,k$-method in more detail, we record the (loss of) fidelity during the execution of Shor's quantum algorithm as a function of time. The

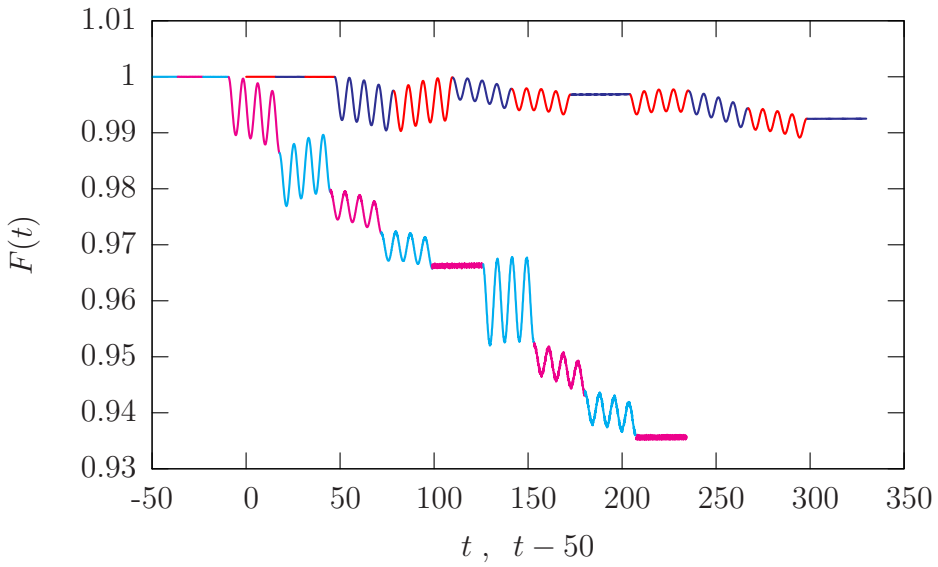


Figure 3: The fidelity, Eq. (21), during the quantum factorization algorithm as a function of time $t$. We show two cases: $\Omega = \Omega_{\Delta}^{(2)} = 0.1$ for $\Delta = 2J'$ (red and blue lines), and $\Omega = 0.116$ (light blue and pink lines), where the fidelity of the final state has a minimum (see Fig. 2). For each case, we used alternating colors to distinguish the individual pulses in the pulse sequence Eqs. (17–19). For better visibility, the curve for $\Omega = 0.116$ is shifted to the left by 50 time units.

result is shown for two cases, $\Omega = \Omega_{\Delta}^{(2)} = 0.1$ for $\Delta = 2J'$, and $\Omega = 0.116$ in Fig. 3. In the first case, the Rabi frequency is a optimal one, according to Eq. (13), whereas in the second case, the Rabi frequency is such that $F_{\rm fi}$, as plotted in Fig. 2 has a minimum. In both cases, we see the expected Rabi oscillations (in $F(t)$) during the majority of the $\pi$-pulses. In the first case, the oscillations are completed during the $\pi$-pulses, such that $F(t)$ at the end of a $\pi$-pulse is almost returns to the value it had at the beginning of the pulse. By contrast, in the second case, the $\pi$-pulses stop when $F(t)$ is almost exactly in a minimum of the near-resonant Rabi oscillations. In the graph of the second case (light blue and pink lines) we can see that for some pulses (*e.g.* the 8'th and the 11'th) there are apparently no oscillations, only a striking broadening of the curve for $F(t)$. During those pulses, the near-resonant transitions with $\Delta = 2J'$ involve states which almost unoccupied, such that the transitions cannot really take place. In those instances we have a chance to see the effects of transitions with $\Delta$ being of the order of $2J$. The resulting oscillations in $F(t)$ are too fast to be resolved, such that the only visible effect is a broadening of the curve. This also demonstrates that the transitions with detuning of the order of $2J$ can be neglected at small Rabi frequencies. That explains the smooth behavior of $F_{\rm fi}(\Omega)$, depicted in Fig. 2.

# 5 Quantum teleportation on 3-qubits

The basic idea of quantum teleportation (Bennett et al. 1993) is that Alice (left end qubit in our chain of three qubits) and Bob (the other end qubit) share two qubits which are in a maximally entangled (Bell) state. Here, we shall follow the prescription of (Nielsen and Chuang 2000).

$$\Phi_{\rm e} = \frac{1}{\sqrt{2}} \left( |0_{\rm A}00_{\rm B}\rangle + |1_{\rm A}01_{\rm B}\rangle \right) . \tag{22}$$

We adjoin to Alice the arbitrary state

$$\Phi_{\rm x} = C_0^{\rm x}|0\rangle + C_1^{\rm x}|1\rangle \ , \tag{23}$$

to be "teleported" to Bob. This results in the quantum state ($\Phi_1 = \Phi_{\rm x} \otimes \Phi_{\rm e}$) of the whole system

$$\Phi_1^{\rm (ideal)} = \frac{1}{\sqrt{2}} \left( C_0^{\rm x} \, |0000\rangle + C_0^{\rm x} \, |0101\rangle + C_1^{\rm x} \, |1000\rangle + C_1^{\rm x} \, |1101\rangle \right) . \tag{24}$$

Then, we apply a controlled-Not (CN) operation between the added qubit and that of Alice

$$\widehat{\rm CN}_{32} \, |i_3, i_2, i_1, i_0\rangle = |i_3, i_2 \oplus i_3, i_2, i_0\rangle \ , \tag{25}$$

where $i_2 \oplus i_3 = (i_2 + i_3) \mathrm{mod}\ 2$. This results in the state

$$\Phi_2^{(\mathrm{ideal})} = \frac{1}{\sqrt{2}} \left( C_0^{\mathrm{x}} \left|0000\right\rangle + C_0^{\mathrm{x}} \left|0101\right\rangle + C_1^{\mathrm{x}} \left|1100\right\rangle + C_1^{\mathrm{x}} \left|1001\right\rangle \right) . \tag{26}$$

In (Nielsen and Chuang 2000) a final Hadamard gate is applied to the added qubit. It allows Alice to measure the two qubits in the computational basis instead of the Bell basis; see (Bennett et al. 1993). In our implementation, we replace the Hadamard gate with a different $\pi/2$-qubit rotation $\widehat{\mathrm{A}}$, which however achieves the same goal:

$$\widehat{\mathrm{A}}_3 \begin{cases} \left|0000\right\rangle \\ \left|1000\right\rangle \end{cases} = \frac{1}{\sqrt{2}} \begin{cases} \left|0000\right\rangle - \left|1000\right\rangle \\ \left|0000\right\rangle + \left|1000\right\rangle \end{cases} . \tag{27}$$

On the Bloch-sphere, this corresponds to a rotation about the angle $-\pi/2$ around the $y$-axis. After some rearrangements, the final state $\Phi_3^{(\mathrm{ideal})} = \widehat{\mathrm{A}}_3 \, \Phi_2^{(\mathrm{ideal})}$ reads:

$$\begin{aligned} \Phi_3^{(\mathrm{ideal})} = \frac{1}{2} \big\{ & \left|00\right\rangle \otimes \left|0\right\rangle \left( C_0^{\mathrm{x}} \left|0\right\rangle + C_1^{\mathrm{x}} \left|1\right\rangle \right) + \left|01\right\rangle \otimes \left|0\right\rangle \otimes \left( C_0^{\mathrm{x}} \left|1\right\rangle + C_1^{\mathrm{x}} \left|0\right\rangle \right) \\ & + \left|10\right\rangle \otimes \left|0\right\rangle \otimes \left( C_1^{\mathrm{x}} \left|1\right\rangle - C_0^{\mathrm{x}} \left|0\right\rangle \right) + \left|11\right\rangle \otimes \left|0\right\rangle \otimes \left( C_1^{\mathrm{x}} \left|0\right\rangle - C_0^{\mathrm{x}} \left|1\right\rangle \right) \big\} . \end{aligned} \tag{28}$$

When Alice measures both of her qubits, there are four possible cases: $\left|00\right\rangle$, $\left|01\right\rangle$, $\left|10\right\rangle$, and $\left|11\right\rangle$. For each case, Bob will get the original state $\Phi_{\mathrm{x}}$, provided he applies the proper operation to his qubits. The operation he has to choose depends on the outcome of Alice's measurement as follows:

| Alice's result | Bob's operation |
|---|---|
| $\left\|00\right\rangle$ | $\widehat{\mathrm{id}}$ |
| $\left\|01\right\rangle$ | $\widehat{\mathrm{N}}$ |
| $\left\|10\right\rangle$ | $-\sigma_z$ |
| $\left\|11\right\rangle$ | $\widehat{\mathrm{N}}\,\sigma_z$ |

where $\widehat{\mathrm{id}} : \left|0\right\rangle \to \left|0\right\rangle , \ \left|1\right\rangle \to \left|1\right\rangle$
$\widehat{\mathrm{N}} : \left|0\right\rangle \to \left|1\right\rangle , \ \left|1\right\rangle \to \left|0\right\rangle$
$\sigma_z : \left|0\right\rangle \to \left|0\right\rangle , \ \left|1\right\rangle \to -\left|1\right\rangle$ . (29)

Note that neither Alice nor Bob need to know the state $\Phi_{\mathrm{x}}$ in order to perform the transfer to Bob's qubit. In fact if any of the two "knew" something about the state, the state transfer would not work.

In order to implement the quantum teleportation scheme on our Ising spin chain quantum computer, we start with a spin chain of 4 spins $(0, \ldots 3)$, where spin 3 is in the unknown state $\Phi_{\mathrm{x}}$.

$$\Phi_0 = C_0^{\mathrm{x}} \left|0000\right\rangle + C_1^{\mathrm{x}} \left|1000\right\rangle . \tag{30}$$

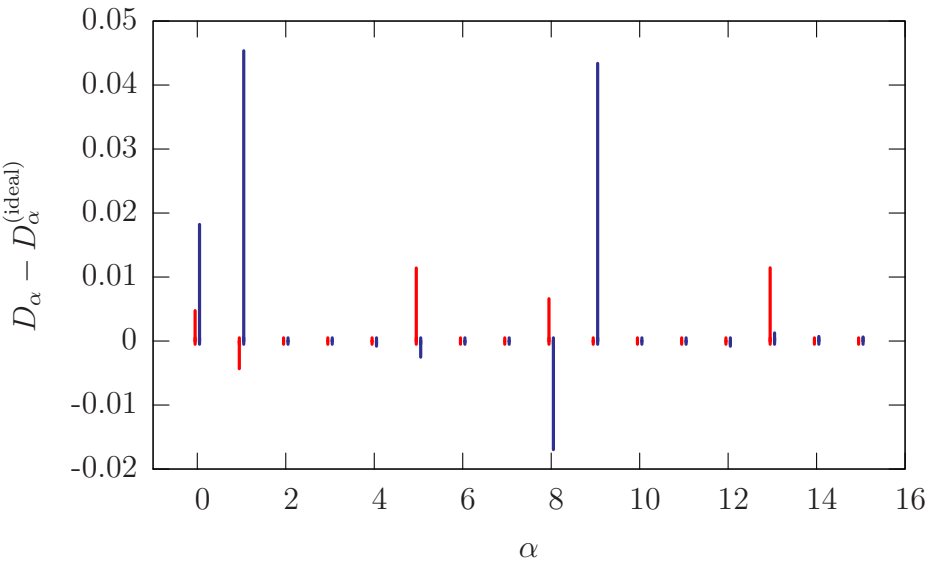


Figure 4: The difference in the expansion coefficients between the final state $\Phi_3$ obtained from the evolution with the full Hamiltonian and the ideal final state $\Phi_3^{(\mathrm{ideal})}$. Red impulses (towards the left) show the real part, blue impulses (towards the right) the imaginary part. The difference in the expansion coefficients is plotted versus $\alpha$, which labels the basis states.

The first step consists in generating an entangled (Bell) state between qubit 2 (Alice) and qubit 0 (Bob). This is obtained with the following three pulses:

$$\Phi_1 = R_0^{1,-1}(\pi, -\pi/2)\; R_2^{0,1}(\pi/2, -\pi/2)\; R_2^{2,1}(\pi/2, -\pi/2)\; \Phi_0\;. \tag{31}$$

Then the controlled-not operation $\widehat{\mathrm{CN}}_{32}$ is applied through

$$\Phi_2 = R_2^{0,-1}(\pi, -\pi/2)\; R_2^{0,1}(\pi, \pi/2)\; \Phi_1\;. \tag{32}$$

The final state, given in Eq. (28), is obtained after applying the $\widehat{A}_3$ to qubit 3 via the following two pulses:

$$\Phi_3 = R_3^{-1,1}(\pi/2, -\pi/2)\; R_3^{1,1}(\pi/2, -\pi/2)\; \Phi_2\;. \tag{33}$$

As an example, we choose $C_0^{\mathrm{x}} = 1/3$ and $C_1^{\mathrm{x}} = \sqrt{8}/3$ for the coefficients of the unknown state.

Again, we simulate the pulse sequence with our model Hamiltonian of Eq. (4) using the parameters of Eq. (7), just as in the previous section. Fig. 4 shows the difference between the final state $\Phi_3$, obtained from the simulation and the ideal final state $\Phi_3^{(\mathrm{ideal})}$, given in Eq. (28). The figure is produced exactly in the same way, as Fig. 1 for the case of Shor factorization.

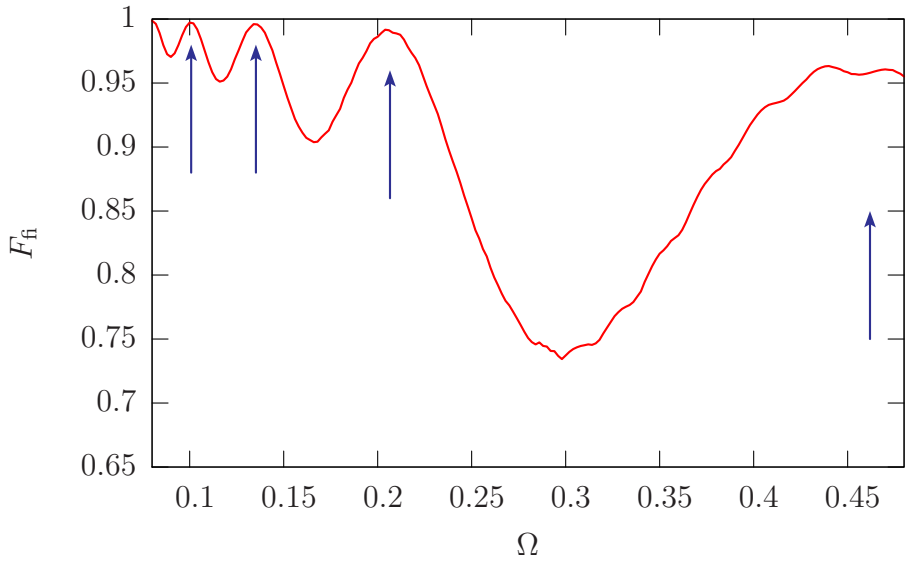


Figure 5: The fidelity, Eq. (21), for the final state resulting from the teleportation algorithm as a function of the Rabi frequency $\Omega$. The blue arrows show the optimal Rabi frequencies $\Omega_\Delta^{(k)}$ according to Eq. (13), for $\Delta = 2J'$ and $k = 1, 2, 3$, and 4 (from right to left).

Here, we find somewhat smaller deviations than in Fig. 1, which may be simply explained by the number of pulses for the teleportation protocol being smaller.

In Fig. 5 we show the fidelity $F_{\rm fi} = |\langle \Phi_3^{(\rm ideal)} | \Phi_3 \rangle|^2$ as a function of the Rabi frequency $\Omega$. Again, Fig. 5 is the precise analog of Fig. 2, where the same quantity is plotted for the Shor factorization protocol. We again find the expected maxima at those points, where the $2\pi\, k$-relation, Eq. (13), is fulfilled. At least for sufficiently small frequencies, there are no noticeable effects of the nearest neighbor interaction, which implies much larger detuning $\Delta \sim 2J$. The present protocol contains $\pi$-pulses, as well as $\pi/2$-pulses. However, note that for $\pi/2$-pulses, the $2\pi\, k$-relation is fulfilled for even $k$, only – see discussion below Eq. (13). On Fig. 5, the corresponding frequencies are marked by the second and the forth arrow, respectively (counting from the right). The data does not show any modulation with respect to $k$ being odd or even. This is a clear signature that the fidelity of the present protocol is largely determined by the $\pi$-pulses alone.

Fig. 6 shows the (loss of) fidelity during the execution of the teleportation protocol as a function of time. In the present case, we choose $\Omega = \Omega_\Delta^{(2)} = 0.1$ for $\Delta = 2J'$. Thus, the Rabi frequency fulfills the $2\pi\, k$-relation, Eq. (13), such that the final fidelity is maximal, locally (see Fig. 5). In Fig. 6 we can distinguish the $\pi/2$ pulses (two on each side) surrounding the three

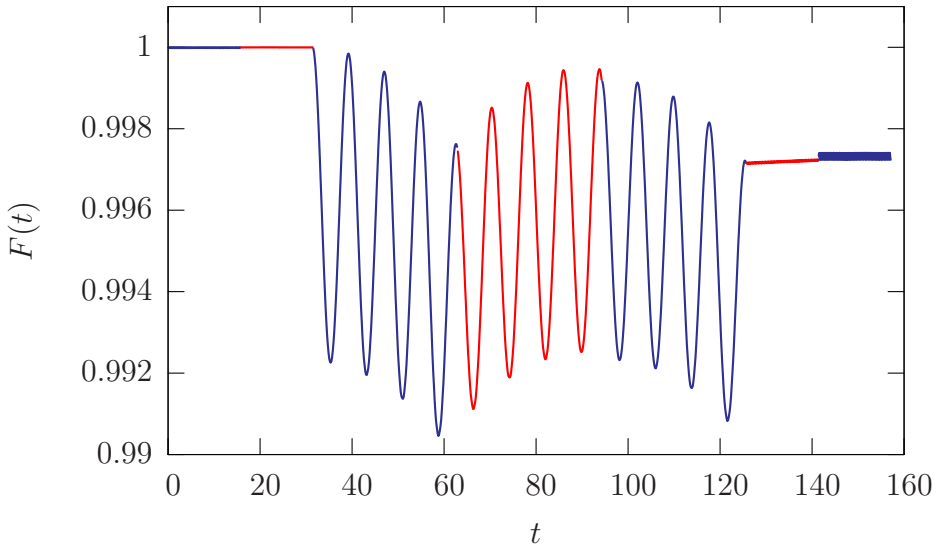


Figure 6: The fidelity, Eq. (21), during the quantum factorization algorithm as a function of time $t$ for $\Omega = \Omega_{\Delta}^{(2)} = 0.1$, where $\Delta = 2J'$ (red and blue lines). We used alternating colors to distinguish the individual pulses in the pulse sequence Eqs. (31–33).

$\pi$-pulses in the middle of the pulse sequence. Oscillations are visible only during the central $\pi$-pulses, not during any of the $\pi/2$-pulses. Note, however that during the last $\pi/2$-pulse we find very fast oscillations with a relatively small amplitude, which must come from detuning of the order of $\Delta \sim 2J$. The behavior of $F(t)$ clearly demonstrates that the loss of fidelity occurs almost exclusively during the execution of the $\pi$-pulses.

# 6 Conclusion

For a quantum computer realized with a one-dimensional chain of nuclear spins (one half), we have studied the effect of an additional second neighbor Ising interaction. This allows greater flexibility in the choice of appropriate pulse sequences for the implementation of a given quantum algorithm. We have found that after adapting the $2\pi k$-method to this new situation, the desired gate operations can be realized with high fidelity. We have illustrated our results with two case studies: Shor's quantum algorithm for the factorization of an integer number, and another algorithm which allows the teleportation of a qubit across the spin chain. In both cases, we have studied the fidelity of the whole algorithm as a function of the Rabi frequency, as well as the decay of fidelity during the algorithm as a function of time. In spite of the fact that both algorithms contain $\pi$- and $\pi/2$-pulses, we found that only the $\pi$-pulses were responsible for the decay of fidelity. We found also that as long as the nearest-neighbor interaction $J$ is much larger than that of the next-nearest neighbor interaction $J'$, the (loss of) fidelity is dominated by the latter. In other words, if the second neighbor interaction in a chain of nuclear spins is not entirely negligible, it will typically dominate the non-resonant effects.


# Acknowledgements

This work was supported by SEP under the contract PROMEP/103.5/04/1911 and the University of Guadalajara.


# A Numerical solution of the Schrödinger equation

We consider the time evolution of the quantum state $\Psi(t)$ of the Ising spin chain during a RF pulse as defined in Eq. (4). The Schrödinger equation reads:

$$\mathrm{i}\hbar\,\partial_t\,\Psi(t) = H(t)\,\Psi(t) \qquad H(t) = H_0 - \frac{\hbar\Omega}{2}\sum_{k=1}^{n}\left(\mathrm{e}^{\mathrm{i}(wt+\varphi)}\,I_k^+ + \mathrm{e}^{-\mathrm{i}(wt+\varphi)}\,I_k^-\right)\,, \tag{34}$$

where $\Psi(0)$ is the quantum state at the beginning of the pulse, and $\Psi(\tau)$ is the state at the end ($\tau$ is the duration of the pulse). The unperturbed Hamiltonian $H_0$ is given in Eq. (2). Expanding $\Psi(t)$ in the basis of the time-independent part $H_0$, we arrive at the matrix form of the Schrödinger equation:

$$\mathrm{i}\partial_t\, C_\alpha(t) = \frac{E_\alpha}{\hbar}\, C_\alpha(t) - \frac{\Omega}{2}\sum_{k=0}^{n-1} \begin{cases} \mathrm{e}^{\mathrm{i}(wt+\varphi)}\, C_{\alpha|\alpha_k=1}(t) & : \alpha_k = 0 \\ \mathrm{e}^{-\mathrm{i}(wt+\varphi)}\, C_{\alpha|\alpha_k=0}(t) & : \alpha_k = 1 \end{cases} . \tag{35}$$

In order to obtain the dynamics in the interaction picture, we set

$$C_\alpha = D_\alpha\, \mathrm{e}^{-\mathrm{i}E_\alpha t/\hbar} \quad \Rightarrow \quad \mathrm{i}\partial_t\, D_\alpha(t) = -\frac{\Omega}{2}\sum_{k=0}^{n-1} \begin{cases} \mathrm{e}^{\mathrm{i}(\Delta_k t+\varphi)} D_{\alpha|\alpha_k=1}(t) & : \alpha_k = 0 \\ \mathrm{e}^{-\mathrm{i}(\Delta_k t+\varphi)} D_{\alpha|\alpha_k=0}(t) & : \alpha_k = 1 \end{cases} , \tag{36}$$

where

$$\Delta_k = w - w_k - J\left[(-1)^{\alpha_{k+1}} + (-1)^{\alpha_{k-1}}\right] - J'\left[(-1)^{\alpha_{k+2}} + (-1)^{\alpha_{k-2}}\right] , \tag{37}$$

as obtained from Eq. (5). Here, it is understood that $(-1)^{\alpha_l} = 0$ if $l < 0$ or $l > n$. In order to evolve the wave packet numerically, it is convenient to rewrite the system of differential equations in terms of real variables. To that end, we introduce the real variables $X_\alpha(t)$ and $Y_\alpha(t)$ such that $D_\alpha = X_\alpha + \mathrm{i}Y_\alpha$. Then we find:

$$\begin{aligned} \partial_t\, X_\alpha(t) &= \frac{\Omega}{2}\sum_{k=0}^{n-1} \begin{cases} -\sin(\Delta_k t+\varphi)\, X_{\alpha|\alpha_k=1}(t) - \cos(\Delta_k t+\varphi)\, Y_{\alpha|\alpha_k=1}(t) & : \alpha_k = 0 \\ \sin(\Delta_k t+\varphi)\, X_{\alpha|\alpha_k=0}(t) - \cos(\Delta_k t+\varphi)\, Y_{\alpha|\alpha_k=0}(t) & : \alpha_k = 1 \end{cases} \\ \partial_t\, Y_\alpha(t) &= \frac{\Omega}{2}\sum_{k=0}^{n-1} \begin{cases} \cos(\Delta_k t+\varphi)\, X_{\alpha|\alpha_k=1}(t) - \sin(\Delta_k t+\varphi)\, Y_{\alpha|\alpha_k=1}(t) & : \alpha_k = 0 \\ \cos(\Delta_k t+\varphi)\, X_{\alpha|\alpha_k=0}(t) + \sin(\Delta_k t+\varphi)\, Y_{\alpha|\alpha_k=0}(t) & : \alpha_k = 1 \end{cases} . \end{aligned} \tag{38}$$

# References


Bennett, C. H., Brassard, G., Crépeau, C., Jozsa, R., Peres, A., and Wootters, W. K. (1993). Teleporting an unknown quantum state via dual classical and Einstein-Podolsky-Rosen channels. *Physical Review Letters* **70**, 1895–1899.

Berman, G. P., Doolen, G. D., Holm, D. D., and Tsifrinovich, V. I. (1994). Quantum computer on a class of one-dimensional Ising systems. *Physics Letters A* **193**, 444–450.

Berman, G. P., Doolen, G. D., López, G. V., and Tsifrinovich, V. I. (2000). Simulations of quantum-logic operations in a quantum computer with a large number of qubits. *Physical Review A* **61**, 062305:1–7.

Berman, G. P., Borgonovi, F., Izrailev, F. M., and Tsifrinovich, V. I. (2001). Single-pulse preparation of the uniform superpositional state used in quantum algorithms. *Physics Letters A* **291**, 232–236.

[a]Berman, G. P., Kamenev, D. I., Doolen, G. D., López, G. V., and Tsifrinovich, V. I., (2002). Perturbation theory and numerical modeling of quantum logic operations with a large number of qubits. *Contemporary Mathematics* **305**, 13–41.

[b]Berman, G. P., López, G. V., and Tsifrinovich, V. I. (2002). Teleportation in a nuclear spin quantum computer. *Physical Review A* **66**, 042312:1–7.

[c]Berman, G. P., Kamenev, D. I., Kassman, R. B., Pineda, C., and Tsifrinovich, V. I. (2002). Method for implementation of universal quantum logic gates in a scalable Ising spin quantum computer. E-print: quant-ph/0212070.

Celardo, G. L., Pineda, C., and Žnidarič, M. (2005). Stability of the quantum Fourier transformation on the Ising quantum computer. *International Journal of Quantum Information* **3**, 441–462.

García-Ripoll, J. J. and Cirac, J. I. (2003). Spin dynamics for bosons in an optical lattice. *New Journal of Physics* **5**, 76:1–13.

Gorin, T., Prosen, T., Seligman, T. H., and Žnidarič, M. (2006). Dynamics of Loschmidt echoes and fidelity decay. *Physics Reports* **435**, 33–156.

Jones, J. A. (2000). NMR quantum computation: a critical evaluation. *Fortschritte der Physik* **48**, 909–924.

Lloyd, S. (1993). A potentially realizable quantum computer. *Science* **261**, 1569–1571.

Lloyd, S. (1995). Quantum-mechanical computers. *Scientific American* **273**, 140–145.

López, G. V., Quezada, J., Berman, G. P., Doolen, G. D., and Tsifrinovich, V. I. (2003). Numerical simulation of a quantum controlled-not gate implemented on four-spin molecules at room temperature. *Journal of Optics B: Quantum and Semiclassical Optics* **5**, 184–189.

López, G. V. and Lara, L. (2006). Numerical simulation of a controlled-controlled-not (CCN) quantum gate in a chain of three interacting nuclear spins system. *Journal of Physics B: Atomic, Molecular and Optical Physics* **39**, 3897–3904.

Nielsen, M. A. and Chuang, I. L. (2000). Quantum Computation and Quantum Information. (Cambridge University Press, Cambridge).

Peres, A. (1984). Stability of quantum motion in chaotic and regular systems. *Physical Review A* **30**, 1610–1615.

Schumacher, B. (1995). Quantum coding. *Physical Review A* **51**, 2738–2747.

Shor, P. W. (1994). Algorithms for quantum computation: discrete logarithms and factoring. In *Proceedings of the 35th Annual Symposium on Foundations of Computer Science*, pp. 124–134, (IEEE Computer Society, Los Alamitos, CA).

Slichter, C. P. (1996). Principles of Magnetic Resonance. (3rd ed., Springer, Berlin).

Vandersypen, L. M. K., Steffen, M., Breyta, G., Yannoni, C. S., Sherwood, M. H., and Chuang, I. L. (2001). Experimental realization of Shor's quantum factoring algorithm using nuclear magnetic resonance. *Nature* **414**, 883–887.